NASA TM X-98

TECHNICAL MEMORANDUM

X-98

EFFECT OF NOZZLE INLET GEOMETRY ON PERFORMANCE OF A SWIVELED CONVERGENT-DIVERGENT NOZZLE

By Albert J. Pavli

Lewis Research Center
Cleveland, Ohio

NATIONAL AERONAUTICS AND SPACE ADMINISTRATION
WASHINGTON
November 1959

NATIONAL AERONAUTICS AND SPACE ADMINISTRATION

TECHNICAL MEMORANDUM X-98

EFFECT OF NOZZLE INLET GEOMETRY ON PERFORMANCE OF A SWIVELED CONVERGENT-DIVERGENT NOZZLE*

By Albert J. Pavli

SUMMARY

The effects of nozzle inlet design variables on the thrust performance and flow characteristics of a swivelable solid-propellant-type rocket nozzle were investigated to provide missile design information. Also investigated were the effects of various inlet configurations on circulation flow through the swivel gap. The tests were performed on a wood nozzle in an altitude test chamber, using dry unheated compressed air (150 lb/sq in. gage) as the flow medium, with nozzle pressure ratios varying from 6 to 140. None of the inlet configurations investigated had any appreciable effect on thrust performance, whereas several significantly affected the flow coefficient.

INTRODUCTION

In order to provide design information for a swivel-type nozzle, an investigation was conducted at the NASA Lewis Research Center to evaluate the effects on nozzle performance of several nozzle geometrical factors. These geometrical factors were representative of certain aerodynamic compromises that might have to be considered in order to satisfy some materials, structures, and heat-transfer criteria.

For the investigation, a wooden nozzle model was installed in a nozzle test rig that was supplied with dry unheated compressed air as the flow medium. The investigation was conducted in two phases. The

*Title, Unclassified.

first phase included the determination of the effect of inlet geometrical factors, blast-tube Mach number, and nozzle swiveling on thrust performance. The second phase was directed toward determining the effect of some swivel-notch variables on circulation velocity in the annular swivel seal chamber. This phase of the investigation is of significance because, in an actual rocket, the velocity in the seal chamber must be kept to a minimum in order to limit the convective heat transfer to the seal.

The entire investigation was conducted using a nozzle with a 4.37-inch throat, 13.4 area ratio, and the divergent contour designed by the method described in reference 1.

APPARATUS

The nozzle test rig (fig. 1) was installed in an altitude test chamber that is connected to the laboratory altitude exhaust system, and the inlet air line was connected to a 150-pound-per-square-inch-gage air supply (approx. 80° F and 1 grain/lb moisture). The pressure ratio was maintained across the nozzle by the labyrinth seal, which allowed the swinging frame and thrust bed to be restrained by the thrust-measuring cell alone. The nozzle contour in the divergent portion was fixed for all the test configurations. A sketch of the nozzle and the static-tap locations, along with coordinates of the contour (both actual and theoretical), appears in figure 2. Also shown by the arrow in figure 2 is the direction of nozzle swiveling relative to the static-tap placement.

The instrumentation on the rig consisted of thermocouples and wall static taps in the inlet air line, total- and static-pressure probes at station 1 (weight-flow-measuring station), total and static probes at station 2 (nozzle inlet station), and static-pressure taps on the wall of the test chamber (station 0, ambient). The pressure taps and thermocouples were connected to the laboratory digital automatic recorder systems.

Diagrams of the models tested in the nozzle performance phase of the program appear in figure 3. Configuration 1 is the standard of comparison, since it has a faired inlet with no irregularities and would be expected to provide the best performance. Configuration 2 was used to find the effect of downstream erosion at a point where the throat lining would end in the divergent section of the actual nozzle. The effect of variations in the plenum approach was determined with

configurations 3 to 5. Blast-tube inlet edge and nozzle swiveling were examined with configurations 6 to 9 for the Mach 0.2 blast tube, and with configurations 10 to 14 for the Mach 0.4 blast tube. The effect of simulated solid-propellant grain to nozzle throat clearance (grain-clearance ratio) when grain port is not in line with nozzle throat was investigated with configurations 15 to 19.

The model used in the circulation-velocity phase of this program is sketched in figure 4, which also illustrates some of the variables investigated. These variables were: blast-tube position swiveled (8°) and unswiveled; blast-tube Mach number (0.2 and 0.4); swivel-notch clearances (0.020 to 0.080 in.); and two sizes of annular grooves (labyrinth-type groove, 5/16 by 1/4 in. deep and 5/16 by 1 in. deep). The effect of these variables on the maximum velocity (which was assumed to occur at the probe location, see fig. 4) was measured with a back-to-back Pitot probe in combination with a wall static tap installed as shown in the figure. The pressure difference across the probe (proportional to ρV^2) was connected to a strain-gage pressure transducer, the output of which was connected through an amplifier to a recording oscillograph; and the wall static tap was connected to the laboratory digital recorder. The entire velocity-probe system was periodically calibrated against a low-speed vane anemometer.

E-582

CH-1 back

PROCEDURE

Prior to the actual nozzle testing, the nozzle test rig was calibrated to determine the effective areas of the two labyrinth seals (one in the inlet air line and the other around the thrust link that passes through the test-chamber wall), the effective area of the force-measuring cell, the inlet momentum force, and the effective flow area at station 1.

In testing the nozzles, each configuration was run over a range of pressure ratio at two inlet pressure levels that were nominally 11,000 and 22,000 pounds per square foot absolute (with the exception of configs. 16 and 17, which were run only at an inlet pressure of 22,000 lb/sq ft abs). Pressure ratio was varied by varying the test-chamber ambient pressure from about 170 to 1900 pounds per square foot absolute, yielding nozzle pressure ratios of about 6 to 140. For each point, measurements were taken on all instrumentation outlined in the APPARATUS section (except velocity probe); and from these measurements the following were calculated: nozzle flow coefficient, $C_{d,3}$; effective thrust coefficient, C_F; thrust coefficient, C_F'; and thrust ratio, F/F_i. (See appendix A for symbols and definitions.)

RESULTS

A general presentation of performance results for each configuration is given in figure 5, in the form of plots of $C_{d,3}$, C_F, and F/F_i against nozzle pressure ratio P_2/p_0. The flow coefficient at station 3 (nozzle throat) $C_{d,3}$, which is the ratio of the effective flow area divided by the actual flow area, indicates the utilization of the physical throat area. The effective thrust coefficient C_F, which is proportional to the measured thrust per unit weight flow, indicates the nozzle's ability to obtain thrust from a given weight flow. The thrust ratio F/F_i is a measure of how close the measured thrust approaches the thrust that is possible theoretically.

On each curve of figure 5, two points are called out, the design point and the separation point. The design point occurs at that pressure ratio P_2/p_0 which will cause the ambient pressure to be equal to the static pressure of the jet at the exit of the nozzle. The separation point occurs at that pressure ratio where flow separation is imminent.

It was determined that the nozzle throat enlarged slightly under pressure; and thus, during the tests, the throat was somewhat larger than when it was measured. Accordingly, flow-coefficient data for several configurations were plotted against air supply pressure, and a correction was determined that was applied to the measured throat area. Thus, when P_2 = 22,000 pounds per square foot absolute, A_3 = 0.10487 square foot; when P_2 = 11,000 pounds per square foot absolute, A_3 = 0.10435 square foot; and when P_2 = 2116 pounds per square foot absolute (atmosphere at sea level), A_3 = 0.10414 square foot.

This correction appeared to be satisfactory for all configurations except configuration 1, which had a flow coefficient slightly greater than unity (1.003) even after the correction was applied, probably because configuration 1 was not as well reinforced as the other configurations and thus expanded more under pressure. It should be noted that any inaccuracies in throat area do not affect the values of F/F_i and C_F, since these parameters are essentially evaluated on a "per unit weight flow" basis, in contrast with C_F', which is essentially evaluated on a "per unit throat area" basis.

In order to present nozzle performance at higher pressure ratios than those experimentally attainable, the data were replotted in a more convenient form. This is shown in figure 6, where C_F' is plotted

against nozzle pressure ratio p_0/P_2 for several typical configurations. The thrust coefficient C_F' is equal to F/P_2A_3. This method of presentation was selected because, when it is employed, the data (for a nozzle that is flowing full) can be represented by a straight line with the slope equal to the physical area ratio (see appendix B). Also, extrapolation of this straight line to p_0/P_2 of zero yields the vacuum thrust coefficient. For all the configurations investigated, the data were adequately represented by straight lines with a constant slope of 13.31. It is to be noted that this value of area ratio (or line slope) is slightly different from that (13.41) noted in figure 2, because it is based on the expanded throat, as previously explained.

A listing of some of the pertinent parameters presented or derivable from figures 5 and 6 appears in table I. Included are values of $C_{d,3}$ from figure 5 and values of C_F' from figure 6. For greater consistency in comparing the data of one configuration with another, the values of C_F and F/F_i presented in table I were calculated from the C_F' curves of figure 6 and the $C_{d,3}$ curves of figure 5 instead of being read directly from figure 5.

DISCUSSION

Blast-Tube Effects

Changes in the blast-tube geometry affected flow coefficient only. The effects on F/F_i and C_F were negligible, as examination of table I will verify. As an aid in selecting the proper values from table I, the following guide is included. To use this guide in finding the effect of blast-tube Mach number, swivel angle, or inlet-edge radius on any tabulated parameter of table I, compare any two configurations that have the same letter in the appropriate column:

Config.	Abbreviation	Blast-tube Mach number	Blast-tube direction	Blast-tube inlet edge
6	0.2-℄-1"R	A	A	A
7	0.2-8°-1"R	B	A	B
11	0.4-℄-1/2"R	-	-	C
10	0.4-℄-1"R	A	B	C
8	0.2-8°-Sq.	C	C	B
12	0.4-8°-1"R	B	B	D
9	0.2-℄-Sq.	D	C	A
13	0.4-℄-Sq.	D	D	C
14	0.4-8°-Sq.	C	D	D

The effects of the blast-tube geometries on $C_{d,3}$ are displayed in figure 7. The effect of blast-tube Mach number on $C_{d,3}$ is essentially independent of nozzle swiveling. The $C_{d,3}$ for the Mach 0.4 tube is lower than that for the 0.2 tube, the difference being about 3.5 percent for square-edged tubes and about 0.8 percent for the 1-inch-radius-edged tubes. In actual rocket-engine applications, the effect of blast-tube Mach number can be counteracted by simply enlarging the nozzle throat diameter, since the magnitude of the effect is relatively constant, being dependent only on blast-tube inlet edge.

The effect of blast-tube inlet-edge radius on $C_{d,3}$ is also independent of nozzle swivel angle. Results for the 1/2-inch-radius inlet were essentially the same as for the 1-inch-radius inlet edge. The difference in $C_{d,3}$ between the square-edged inlet and the 1-inch-radius inlet was about 3.5 percent for the Mach 0.4 blast tube and about 1.0 percent for the Mach 0.2 blast tube, $C_{d,3}$ for the square-edged inlet being lower. Since the magnitude of this effect is dependent only on blast-tube Mach number, it can also be counteracted in actual rocket applications by enlarging the throat diameter.

The effect of swiveling the blast tube relative to the nozzle is less than 1/2 percent on $C_{d,3}$ for 8° swivel, the $C_{d,3}$ being larger for the unswiveled case. In a rocket engine, this would result in 1/2-percent (or less) decrease in nozzle throat effective area and thus a slight increase in thrust. This increased thrust would occur because of the decreased flow area, which causes an increase in chamber pressure and thus an increase in the propellant burning rate and the weight flow through the nozzle.

The static-pressure distribution in the divergent section of the nozzle was investigated in order to determine whether any circumferential pressure asymmetry was caused by the swiveling of the blast tube. Pressure asymmetry in the divergent section is of significance because its presence would cause a yaw force that would have to be allowed for when the nozzle is vectored. Two typical static-pressure distributions extending to area ratios of 3.5 appear in figure 8. These plots were not extended beyond an area ratio of 3.5 because no differences existed beyond this point. Within the accuracy of the instrumentation, nozzle vectoring (or blast-tube swiveling) did not change the circumferential pressure distribution, and hence missile side forces can be readily calculated from the nozzle swivel angle and trigonometric relations.

Grain to Throat Clearance

The effect of grain clearance on nozzle performance is shown in figure 9, which is a plot of nozzle flow coefficient $C_{d,3}$ and thrust ratio $(F/F_i)_{des}$ against grain-clearance ratio L/D_3. Each configuration

had a different design pressure ratio because the effective throat area $C_{d,3}$, and hence the effective area ratio, was different. Therefore, the thrust ratio used in this plot is evaluated at the individual design pressure ratio of each configuration. As grain clearance is increased, both $C_{d,3}$ and $(F/F_i)_{des}$ increase and then remain essentially constant. At a grain-clearance ratio of about 0.6, the $C_{d,3}$ levels out at a value of about 0.968, which is slightly lower than the 0.986 obtained with the same configuration (configs. 10 and 19, see figs. 3(j) and (o)) without the movable bulkhead simulating the grain end with a port opening. The reason for this difference is that approximately a $1\frac{1}{2}$-percent total-pressure loss occurred through the Mach 0.2 opening simulating the grain port, thereby decreasing $C_{d,3}$ $1\frac{1}{2}$ percent. In practical rocket applications, grain-clearance ratios of less than 0.6 would probably be undesirable, because $C_{d,3}$ would continually increase as the grain burned and the geometry in front of the blast tube changed.

Erosion

The erosion notch in configuration 2 had no measurable effect on thrust or airflow characteristics (see table I).

Plenum Approaches

The effect of several plenum approaches (configs. 3, 4, and 5) on both thrust and flow coefficients (see table I) was negligible.

Circulation Velocity

The results of the seal-chamber circulation-velocity test are illustrated in the following table (see fig. 4 for description of config.):

Config.	Abbreviation	Swivel-notch clearance, in.	Annular groove	Circulation velocity, ft/sec
10	0.4-$\frac{1}{8}$-1"R	0.020-0.025	None	-26
12	0.4-8°-1"R	.020-.025	None	+50
7	0.2-8°-1"R	.020-.025	None	+86
12	0.4-8°-1"R	.062-.082	None	+218
12	0.4-8°-1"R	.030-.040	5/16" × 1/4" Deep	+114
12	0.4-8°-1"R	.030-.040	5/16" × 1" Deep	+100

Although seal-chamber circulation is definitely influenced by nozzle swiveling, the values in the preceding table indicate that some circulation velocity existed for the unswiveled case (config. 10, 0.4-$\frac{1}{4}$-1"R) as well. However, the velocity is in the opposite direction from the velocities encountered with swiveled configurations. The reason for this is not known for certain, but slight unintentional configuration asymmetry is suspected.

Flow-circulation data for the Mach 0.4 blast tube swiveled 8° (config. 12) appear in figure 10 as a plot of circulation velocity against swivel-notch clearance. With the nozzle swiveled, circulation velocity varies almost directly with swivel-notch clearance. In addition, it is also apparent that the two labyrinth-type grooves had very little effect.

As can be seen in preceding table, circulation velocity is considerably higher for the Mach 0.2 blast-tube configuration than for the Mach 0.4, probably because the swivel notch is more exposed to the main stream and is not shielded behind the trailing edge of the blast tube as it is for the Mach 0.4 case. Thus, in an actual rocket, seal-chamber circulation velocity, and therefore heat transfer to the seal, can be reduced by (1) reducing the size of the swivel gap, (2) shielding the gap behind the trailing edge of the blast tube, and/or (3) providing a symmetrical inlet (swiveled or unswiveled).

SUMMARY OF RESULTS

The results of an investigation of the effect of inlet geometrical factors such as blast-tube diameter (Mach number), blast-tube inlet radius, nozzle swiveling, and simulated propellant grain to exhaust-nozzle clearance on the performance of a nozzle type applicable to solid-propellant rockets indicated that these factors had negligible effect on nozzle thrust coefficient, whereas the effects on nozzle flow coefficient were more significant. The effects on nozzle flow coefficient are listed in order of decreasing magnitude:

(1) Simulated grain-clearance ratios below 0.65

(2) Blast-tube inlet radius

(3) Blast-tube Mach number (blast-tube diam.)

(4) Swiveling the nozzle (not more than 0.6 % effect)

The results of the investigation of geometric variables on the circulation through the annular seal chamber indicated that seal-chamber circulation velocity was primarily caused by nozzle swiveling and varied approximately linearly with swivel-notch clearance.

Lewis Research Center
National Aeronautics and Space Administration
Cleveland, Ohio, July 27, 1959

E-582

CH-2

APPENDIX A

SYMBOLS

A area

C_d flow coefficient, $\frac{\text{Effective flow area}}{\text{Actual physical area}}$

C_F effective thrust coefficient, $F/P_2A_3C_{d,3}$

C'_F thrust coefficient, F/P_2A_3

$C_{F,i}$ $F_i/P_2A_3C_{d,3}$

D diameter

F measured thrust

$\frac{F}{F_i}$ thrust ratio, $C_F/C_{F,i}$

F_i ideal thrust (thrust obtainable from measured mass flow when expanded isentropically to particular p_0/P_2)

L length

M Mach number

m mass flow

P total pressure

p static pressure

V velocity

ρ density

Subscripts:

des coefficient evaluated at configuration design pressure ratio

e exit

i ideal

vac coefficient evaluated at vacuum (infinite pressure ratio)

0	test chamber (ambient)
1	weight-flow-measuring station
2	nozzle inlet
3	nozzle throat
110	coefficient evaluated at pressure ratio of 110

APPENDIX B

DERIVATION FOR C_F' METHOD OF NOZZLE THRUST DATA EXTRAPOLATION

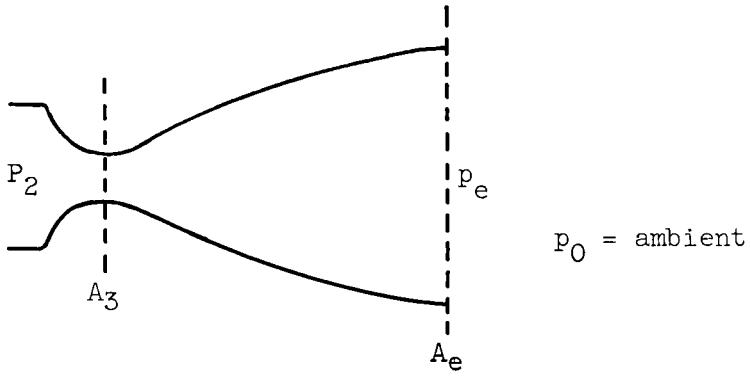

The thrust of a nozzle is

$$F = mV_e + p_eA_e - p_0A_e$$

By definition,

$$C_F' \equiv \frac{F}{P_2A_3}$$

Substituting,

$$C_F' = \frac{mV_e}{P_2A_3} + \frac{p_eA_e}{P_2A_3} - \frac{p_0A_e}{P_2A_3}$$

For a nozzle flowing full (unseparated flow),

$$\frac{mV_e}{P_2A_3} + \frac{p_eA_e}{P_2A_3} = \text{constant} = K_1$$

and

$$C_F' = K_1 - \frac{p_0A_e}{P_2A_3}$$

Taking a first derivative,

$$\frac{dC_F'}{d(p_0/P_2)} = -\frac{A_e}{A_3} = -13.31$$

Hence, C_F' against p_0/P_2 on Cartesian coordinates should plot as a straight line of slope -13.31.

REFERENCE

1. Rao, G. V. R.: Contoured Rocket Nozzles. Paper presented at Ninth Annual Cong. Inst. Astronautical Federation (Amsterdam), Aug. 25-30, 1958.

TABLE I. - RESULTS

Config.	Abbreviation	$C_{a,3}$	$(P_2/P_0)_{des}$	$(P_0/P_2)_{des}$	$C_{F,i,des}$	$C'_{F,vac}$	$C_{F,vac}$	$(F/F_i)_{vac}$	$C'_{F,110}$	$C_{F,110}$	$(F/F_i)_{110}$	$C'_{F,des}$	$C_{F,des}$	$(F/F_i)_{des}$
1	Std.	1.003	110	0.00909	1.5573	1.624	1.618	0.971	1.505	1.500	0.963	1.505	1.500	0.963
2	Erosion	.999	116	.00862	1.5615	1.628	1.627	.975	1.506	1.508	.968	1.511	1.512	.968
6	0.2-ℓ-1"R	.995	115	.00869	1.5608	1.617	1.624	.974	1.495	1.502	.964	1.500	1.507	.965
5	Borda	.991	108	.00925	1.5559	1.618	1.632	.979	1.499	1.513	.971	1.496	1.510	.970
4	Abrupt	.991	122	.00819	1.5654	1.617	1.632	.979	1.498	1.512	.971	1.509	1.522	.972
3	Std.+Notch	.990	115	.00869	1.5608	1.617	1.633	.979	1.496	1.511	.970	1.500	1.515	.971
7	0.2-8°-1"R	.990	117	.00854	1.5622	1.617	1.633	.979	1.498	1.513	.971	1.504	1.519	.972
11	0.4-ℓ-1/2"R	.988	114	.00877	1.5602	1.617	1.636	.981	1.497	1.515	.973	1.501	1.519	.973
10	0.4-ℓ-1"R	.986	114	.00877	1.5602	1.604	1.627	.976	1.484	1.505	.966	1.488	1.509	.967
9	0.2-ℓ-Sq.	.983	118	.00847	1.5628	1.602	1.629	.977	1.483	1.509	.969	1.490	1.516	.970
12	0.4-8°-1"R	.982	119	.00840	1.5634	1.603	1.632	.978	1.483	1.510	.970	1.490	1.517	.970
8	0.2-8°-Sq.	.981	119	.00840	1.5634	1.602	1.633	.980	1.482	1.511	.970	1.490	1.519	.972
19	MB @ 8	.969	119	.00840	1.5634	1.579	1.630	.977	1.459	1.506	.967	1.467	1.514	.968
18	MB @ 2	.957	120	.00833	1.5642	1.557	1.627	.976	1.437	1.502	.964	1.447	1.512	.966
13	0.4-ℓ-Sq.	.952	119	.00840	1.5634	1.554	1.632	.978	1.436	1.508	.968	1.444	1.517	.970
14	0.4-8°-Sq.	.946	123	.00813	1.5659	1.544	1.632	.978	1.424	1.505	.966	1.436	1.518	.969
17	MB @ 1	.925	125	.00800	1.5672	1.509	1.631	.978	1.389	1.502	.964	1.402	1.516	.967
16	MB @ 1/2	.893	127	.00787	1.5684	1.454	1.628	.976	1.334	1.494	.959	1.349	1.511	.963
15	MB @ 1/4	.868	130	.00769	1.5701	1.415	1.630	.977	1.295	1.492	.958	1.312	1.511	.962

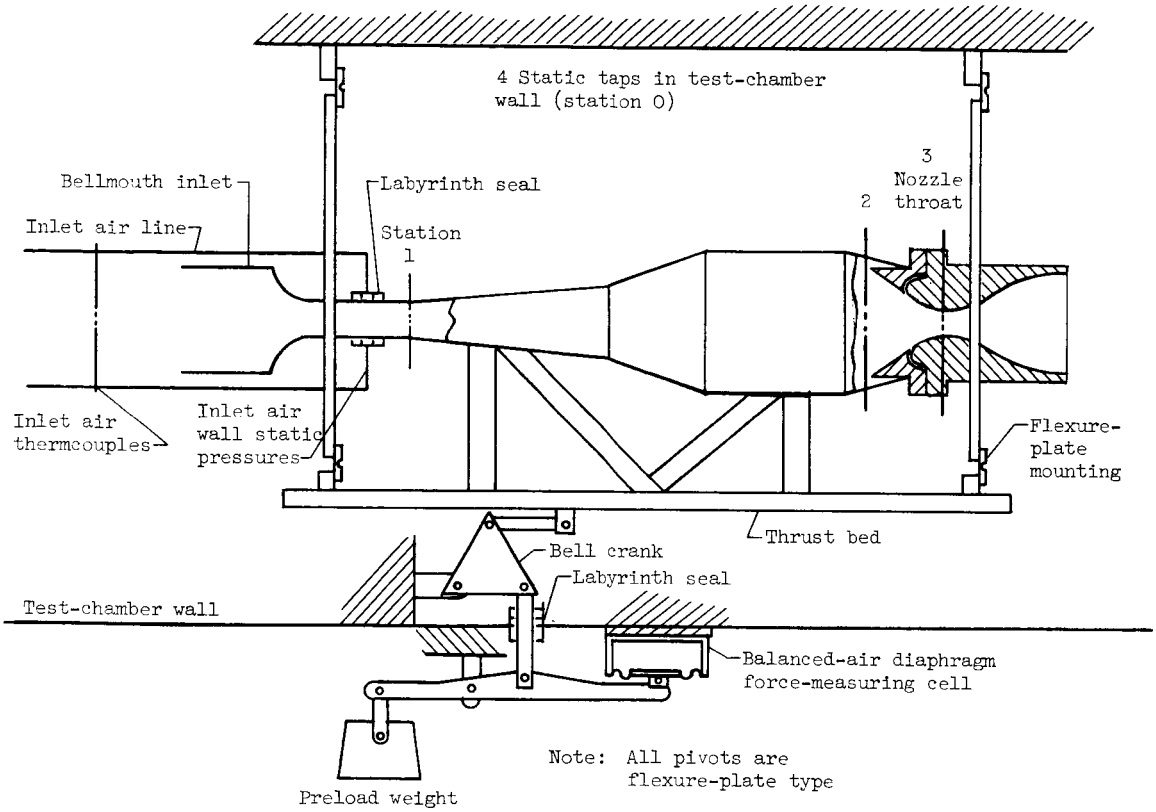

Station	Total probes	Static taps	Boundary rakes
1 (wt. flow)	12	6	3
2 (nozzle inlet)	20	6	1
0 (ambient)	--	4	-

Figure 1. - Sketch of nozzle rig showing location of instrumentation stations.

3 Longitudinal rows of static taps at 90° to each other
13 Taps in each row

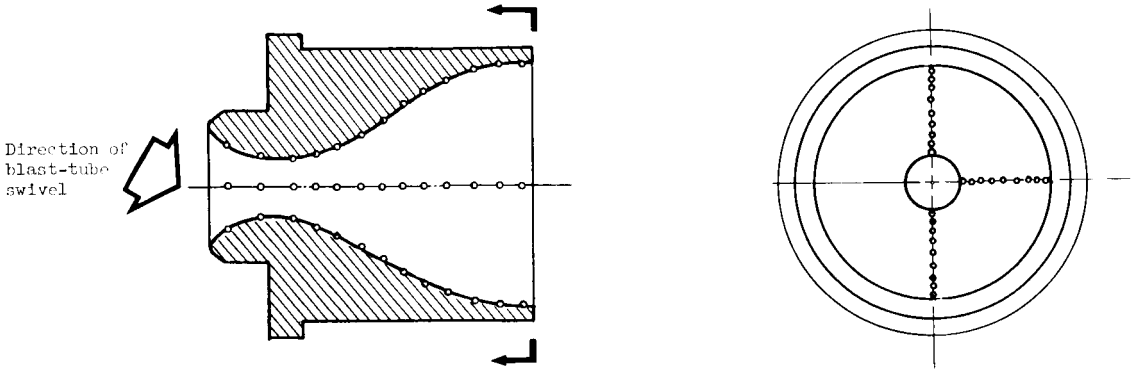

Axial distance from throat, in.	Nominal A/A_3	Actual diameters measured 90° apart, in.		Theoretical diameter, in.
		Top to bottom	Left to right	
-2.8	2.7	------	------	------
-1.7	1.3	------	------	------
0	1.0	4.380	4.363	4.300
1.047	1.3	4.869	4.905	4.840
2.032	1.8	5.837	5.857	5.810
3.016	2.4	6.792	6.804	6.760
4.516	3.5	8.181	8.213	8.130
6.047	4.7	9.473	9.487	9.380
7.610	5.9	10.563	10.638	10.535
10.115	8.0	12.312	12.413	12.180
12.588	9.7	13.563	13.638	13.545
15.113	11.4	14.748	14.763	14.745
17.713	13.1	15.814	15.869	15.625
18.468	13.4	16.003	15.997	16.014

Figure 2. - Sketch of nozzle showing instrumentation and contour coordinates.

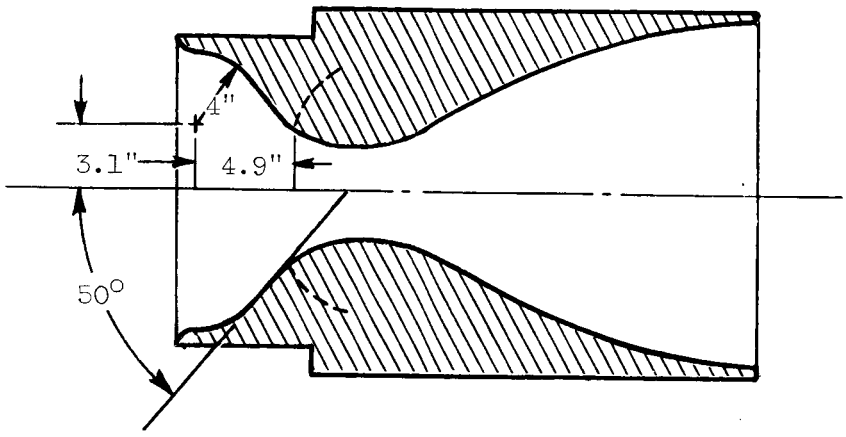

(a) Configuration 1: Standard plenum inlet (Std.).

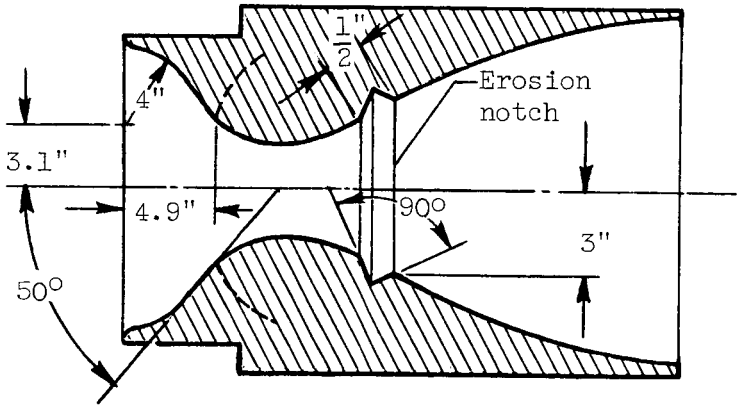

(b) Configuration 2: Standard plenum inlet with erosion notch downstream of throat (Erosion).

Figure 3. - Configuration diagrams.

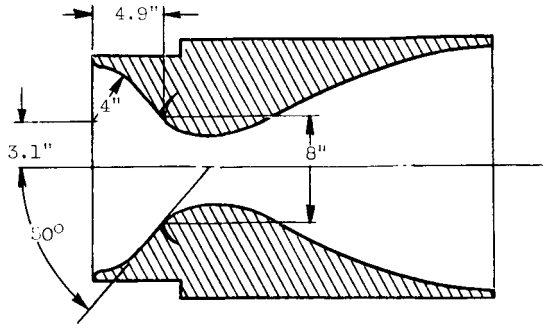

(c) Configuration 3: Standard plenum inlet fairing with characteristic swivel notch at Mach 0.2 (Std.+Notch).

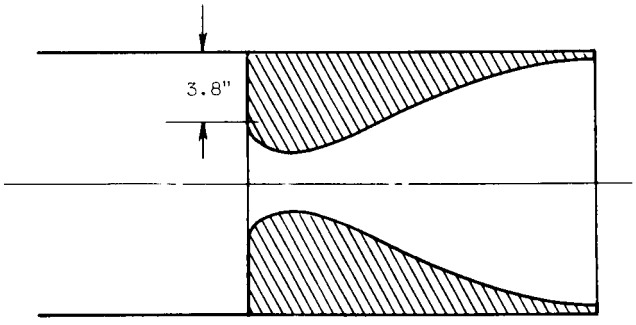

(d) Configuration 4: Abrupt nozzle approach from plenum (Abrupt).

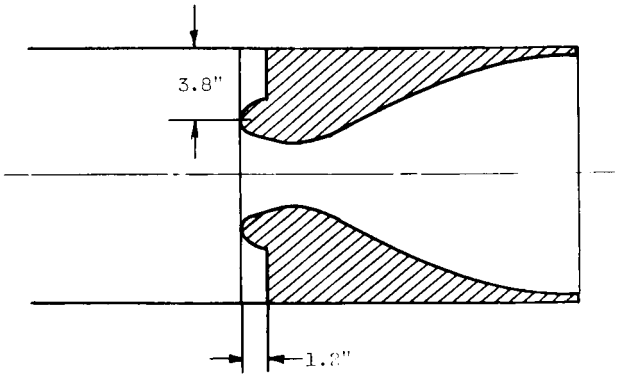

(e) Configuration 5: Borda nozzle approach from plenum (Borda).

Figure 3. - Continued. Configuration diagrams.

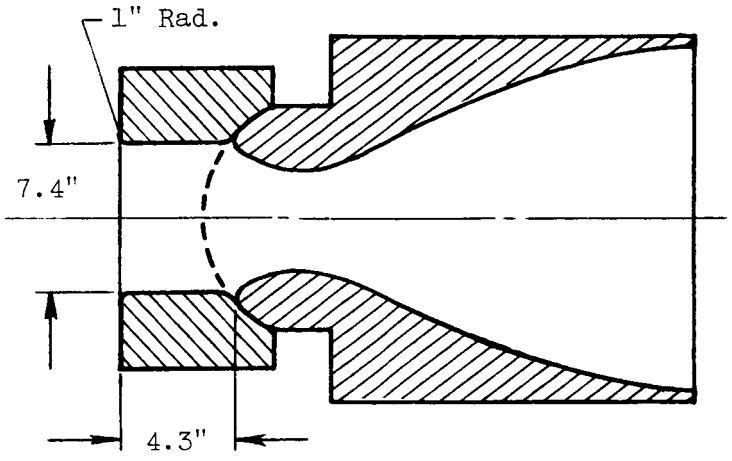

(f) Configuration 6: Mach 0.2 blast tube unswiveled with 1-inch-radius inlet edge (0.2-0-1"R).

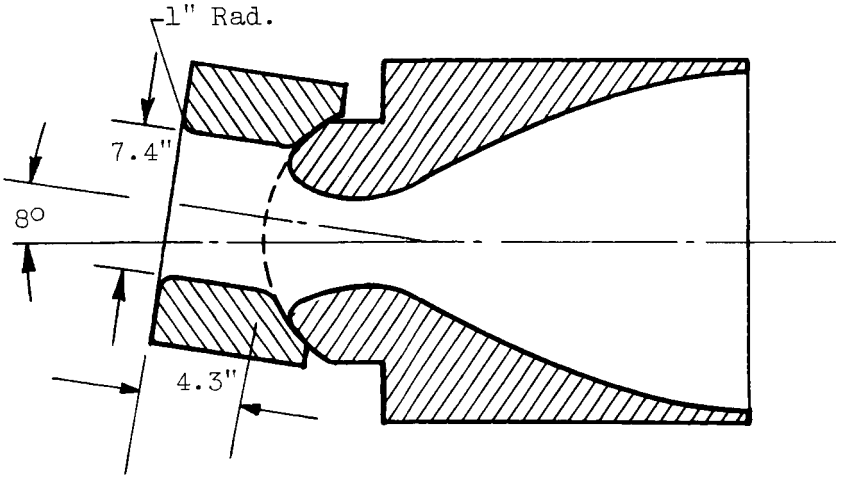

(g) Configuration 7: Mach 0.2 blast tube swiveled at 8° with 1-inch-radius inlet edge (0.2-8°-1"R).

Figure 3. - Continued. Configuration diagrams.

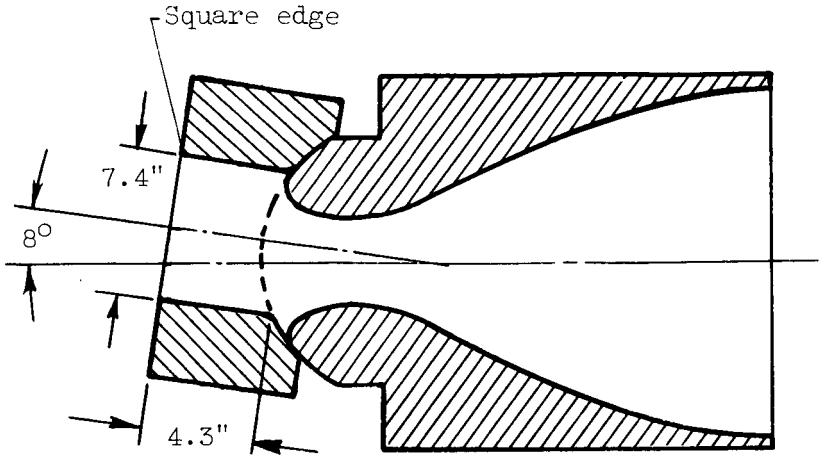

(h) Configuration 8: Mach 0.2 blast tube swiveled 8° with square-edged inlet (0.2-8°-Sq.).

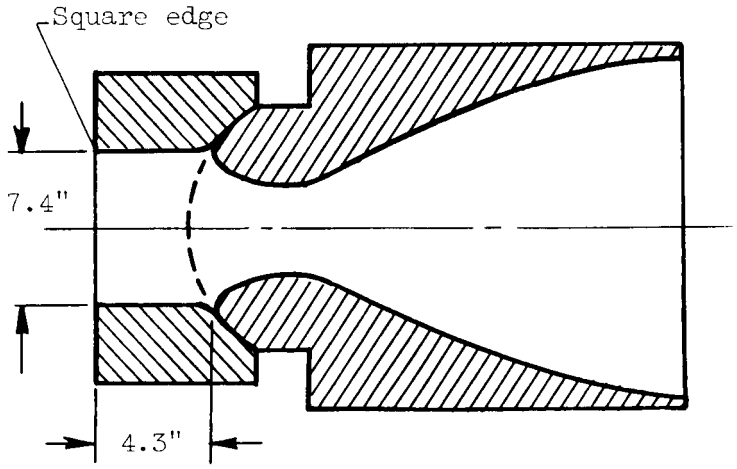

(i) Configuration 9: Mach 0.2 blast tube unswiveled with square-edged inlet (0.2-℄-Sq.).

Figure 3. - Continued. Configuration diagrams.

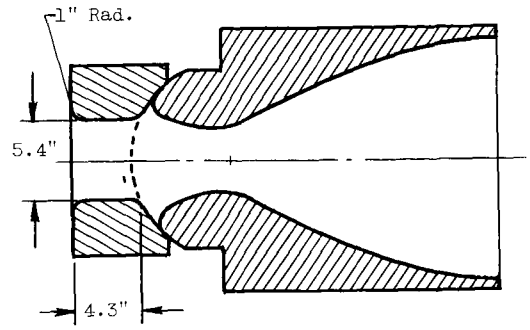

(j) Configuration 10: Mach 0.4 blast tube unswiveled with 1-inch-radius inlet edge (0.4-℄-1"R).

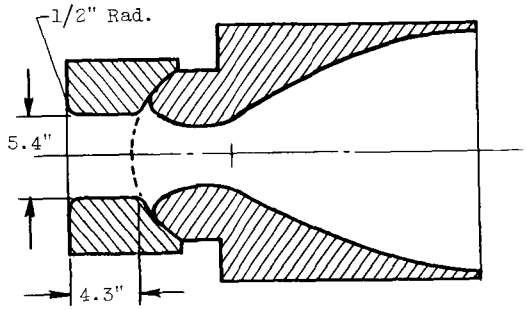

(k) Configuration 11: Mach 0.4 blast tube unswiveled with 1/2-inch-radius inlet edge (0.4-℄-1/2"R).

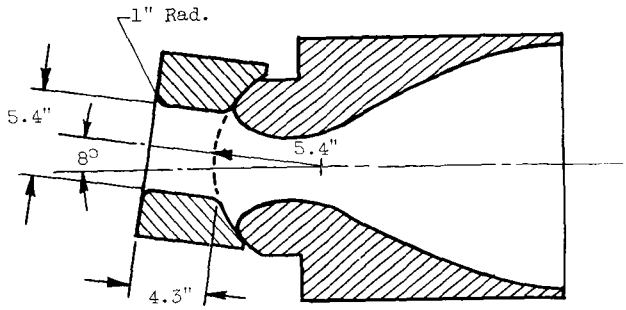

(l) Configuration 12: Mach 0.4 blast tube swiveled at 8° with 1-inch-radius inlet edge (0.4-8°-1"R).

Figure 3. - Continued. Configuration diagrams.

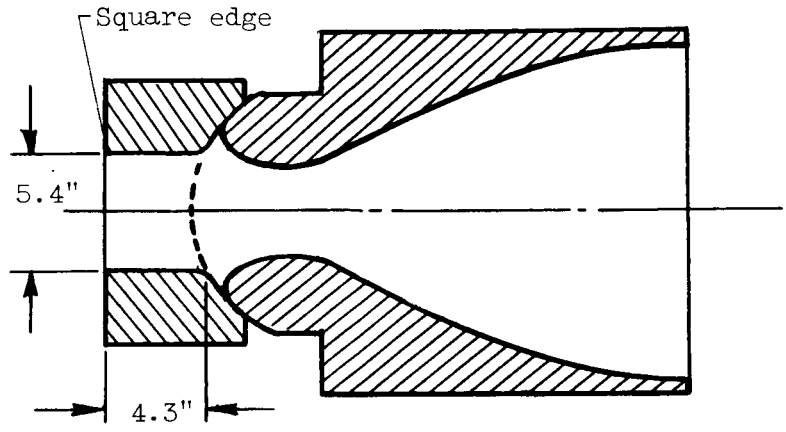

(m) Configuration 13: Mach 0.4 blast tube unswiveled with square-edged inlet (0.4-ℓ-Sq.).

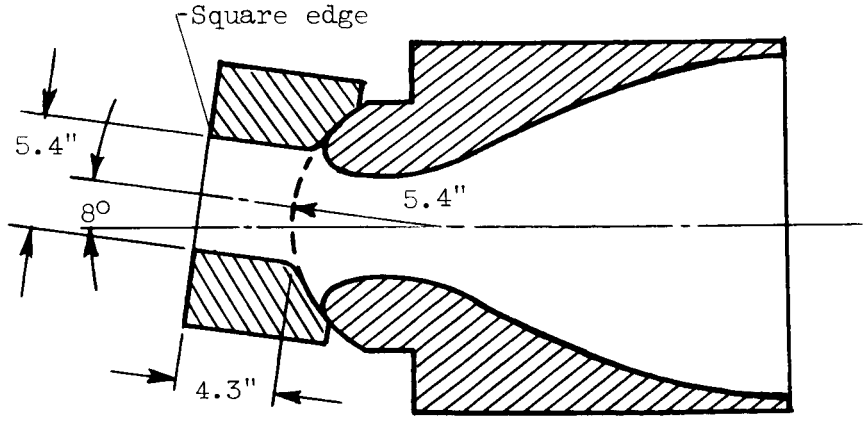

(n) Configuration 14: Mach 0.4 blast tube swiveled at 8° with square-edged inlet (0.4-8°-Sq.).

Figure 3. - Continued. Configuration diagrams.

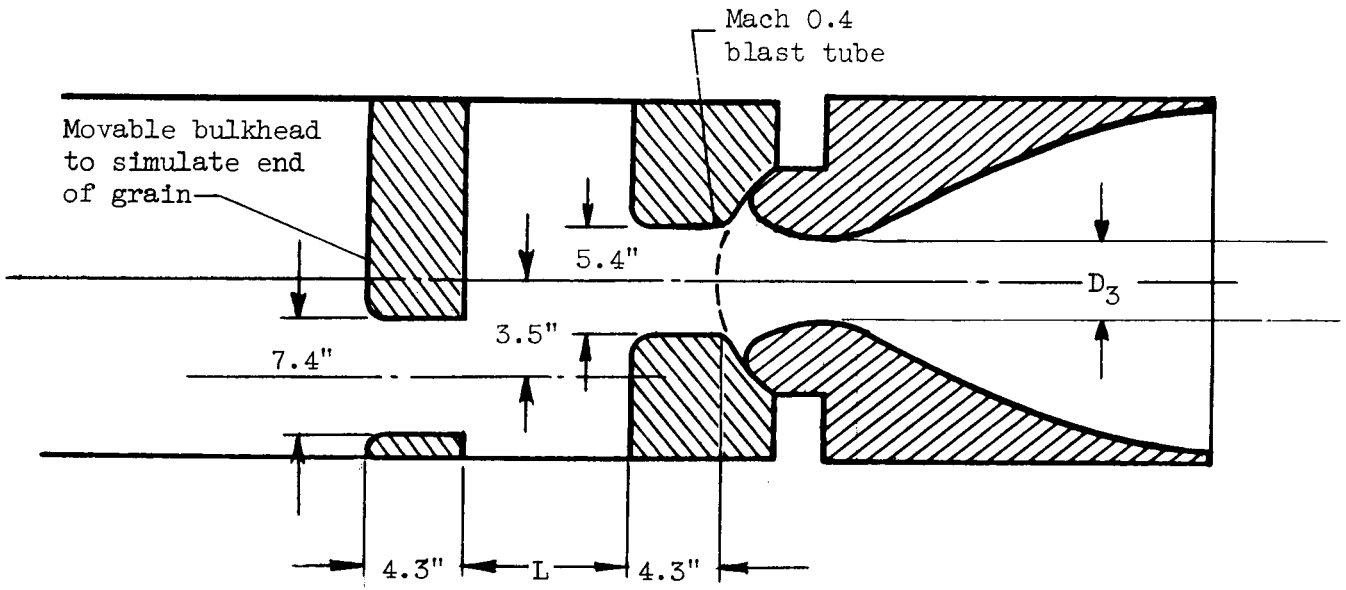

Configuration	Abbreviation	Simulated grain clearance, L, in.	Simulated grain-clearance ratio, L/D_3
15	MB @ 1/4	1/4	0.057
16	MB @ 1/2	1/2	.114
17	MB @ 1	1	.228
18	MB @ 2	2	.456
19	MB @ 6	6	1.372

(o) Movable-bulkhead configurations 15 to 19. (Downstream surface of movable bulkhead to simulate end of port burning grain in a multinozzle, solid-propellant rocket engine.)

Figure 3. - Concluded. Configuration diagrams.

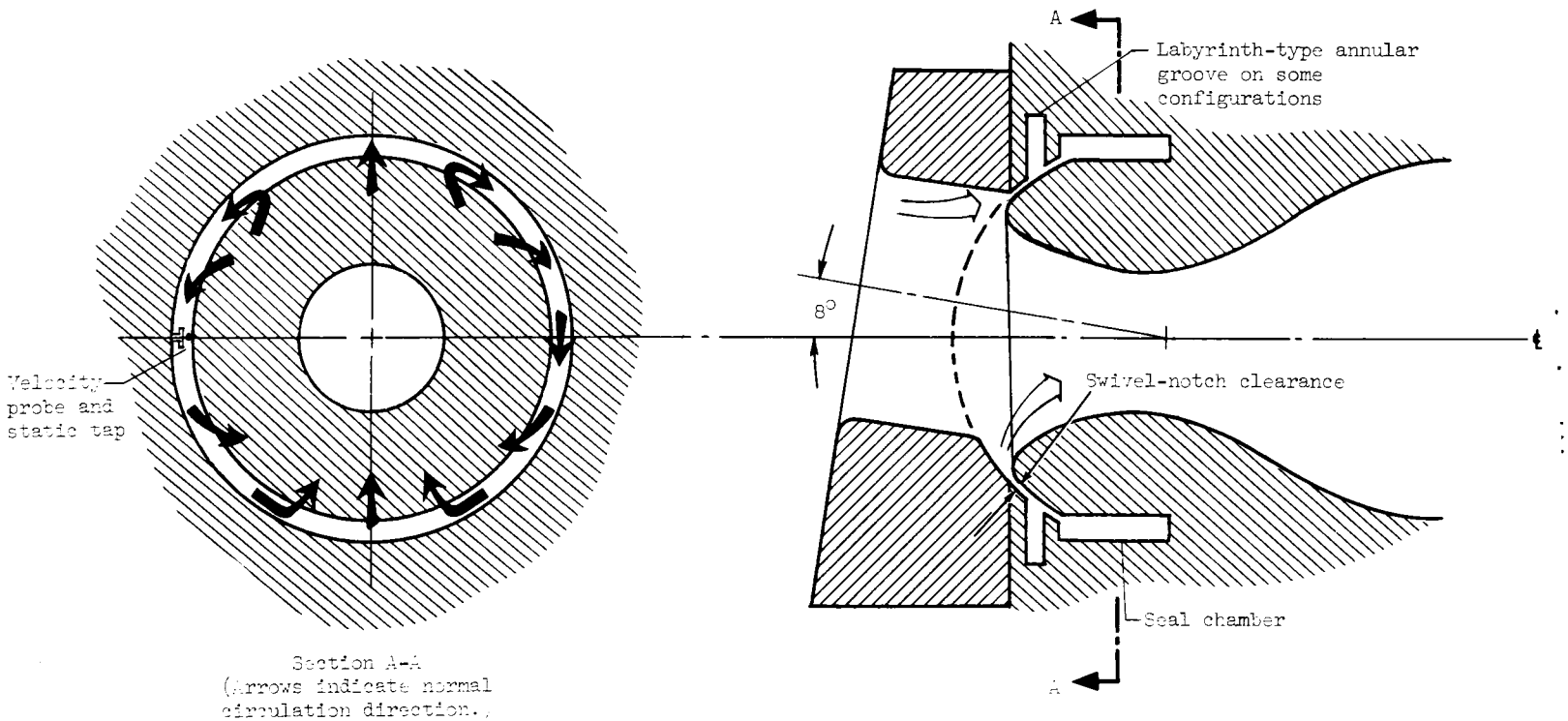

Figure 4. - Sketch of circulation-velocity configuration with instrumentation.

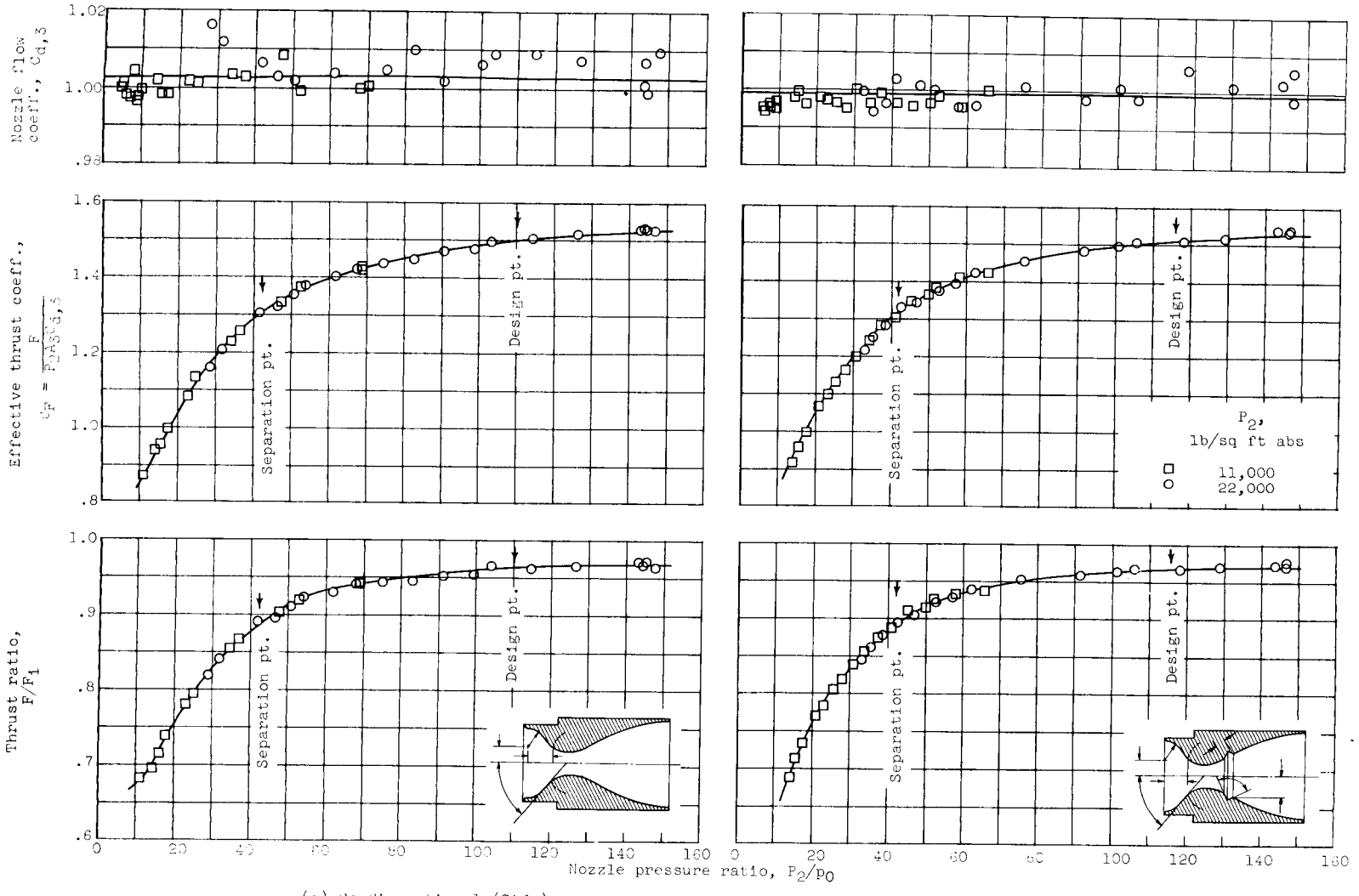

(a) Configuration 1 (Std.).

(b) Configuration 2 (Erosion).

Figure 5. - Variation of $C_{d,3}$, C_F, and F/F_I with pressure ratio P_2/P_0.

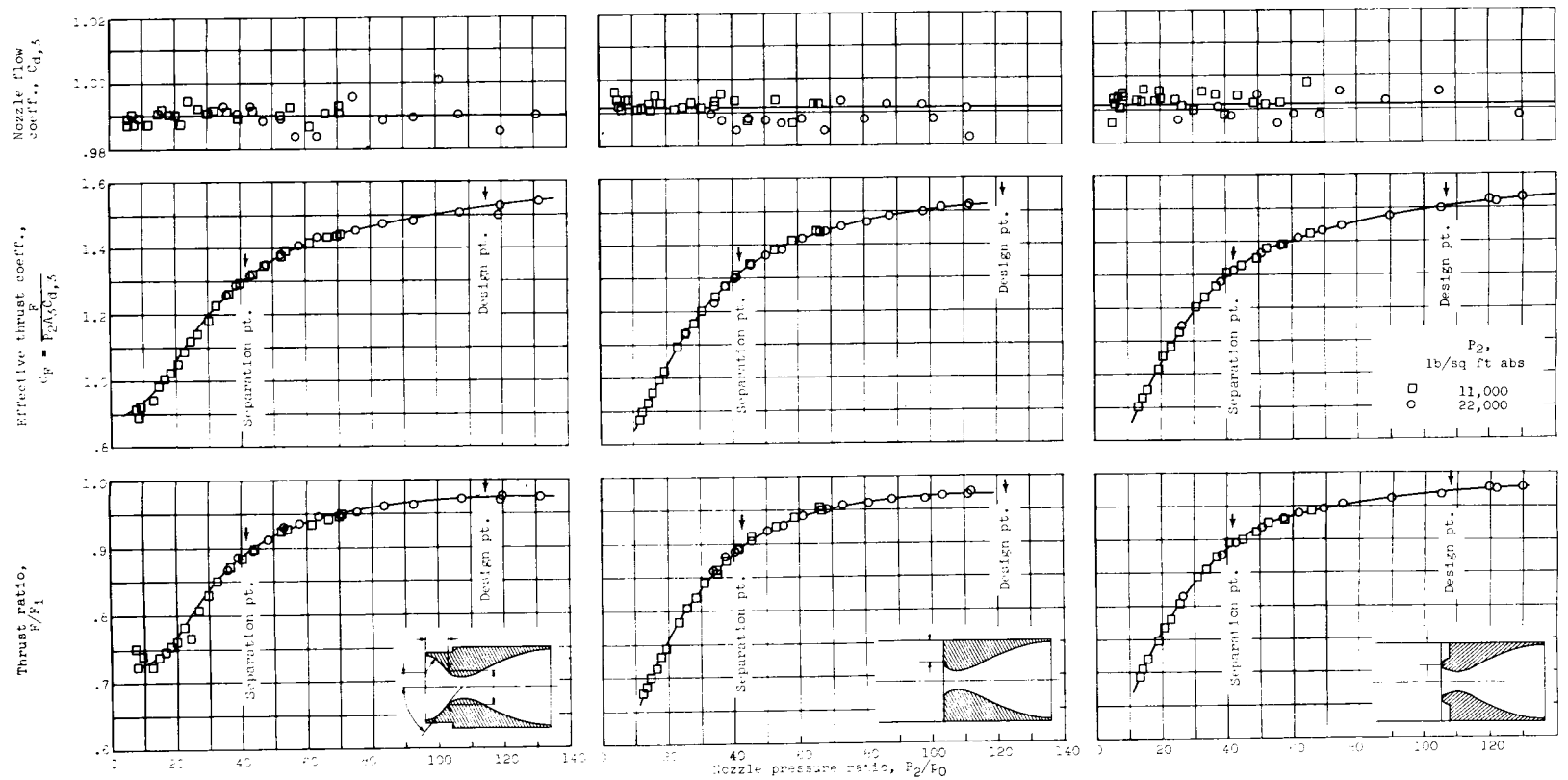

(c) Configuration 3 (Std.+Notch). (d) Configuration 4 (Abrupt). (e) Configuration 5 (Borda).

Figure 5. - Continued. Variation of $C_{d,3}$, C_F, and F/F_1 with pressure ratio P_2/p_0.

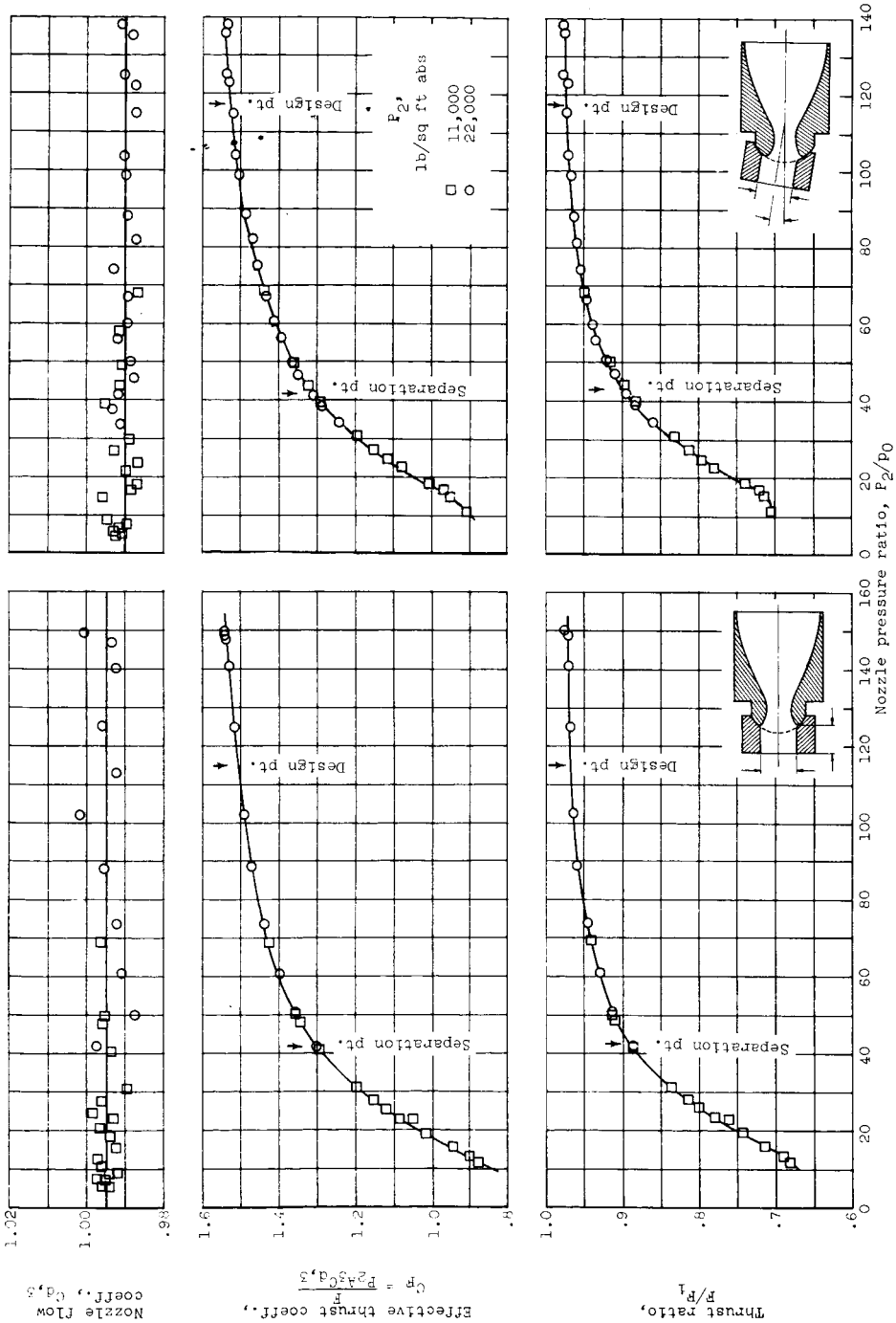

(f) Configuration 6 (0.2-$\frac{1}{2}$-1"R).

(g) Configuration 7 (0.2-8°-1"R).

Figure 5. - Continued. Variation of $C_{d,3}$, C_F, and F/F_1 with pressure ratio P_2/p_0.

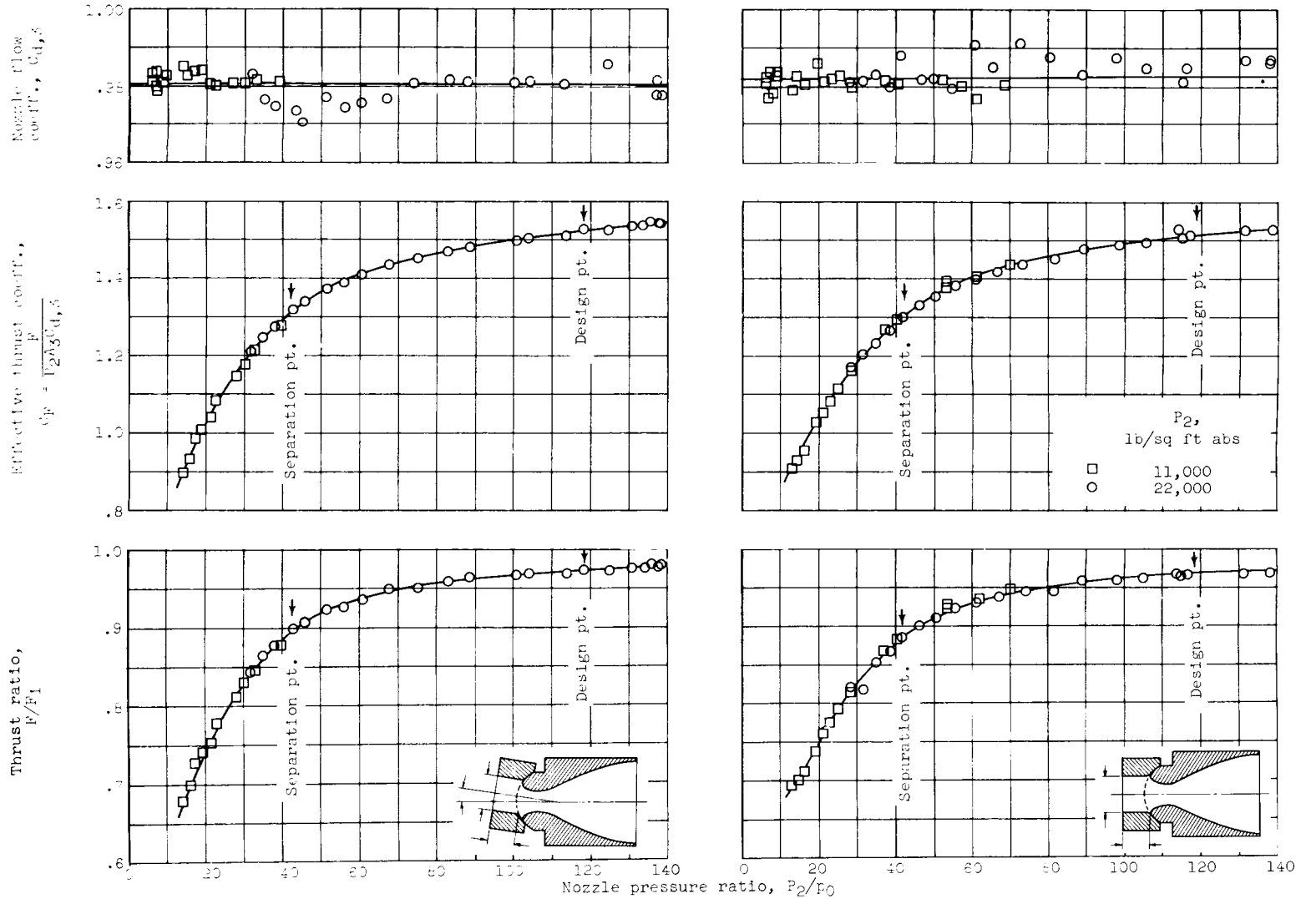

(h) Configuration 8 (0.2-8°-Sq.).

(i) Configuration 9 (0.2-$\frac{1}{4}$-Sq.).

Figure 5. - Continued. Variation of $C_{d,3}$, C_F, and F/F_1 with pressure ratio P_2/p_0.

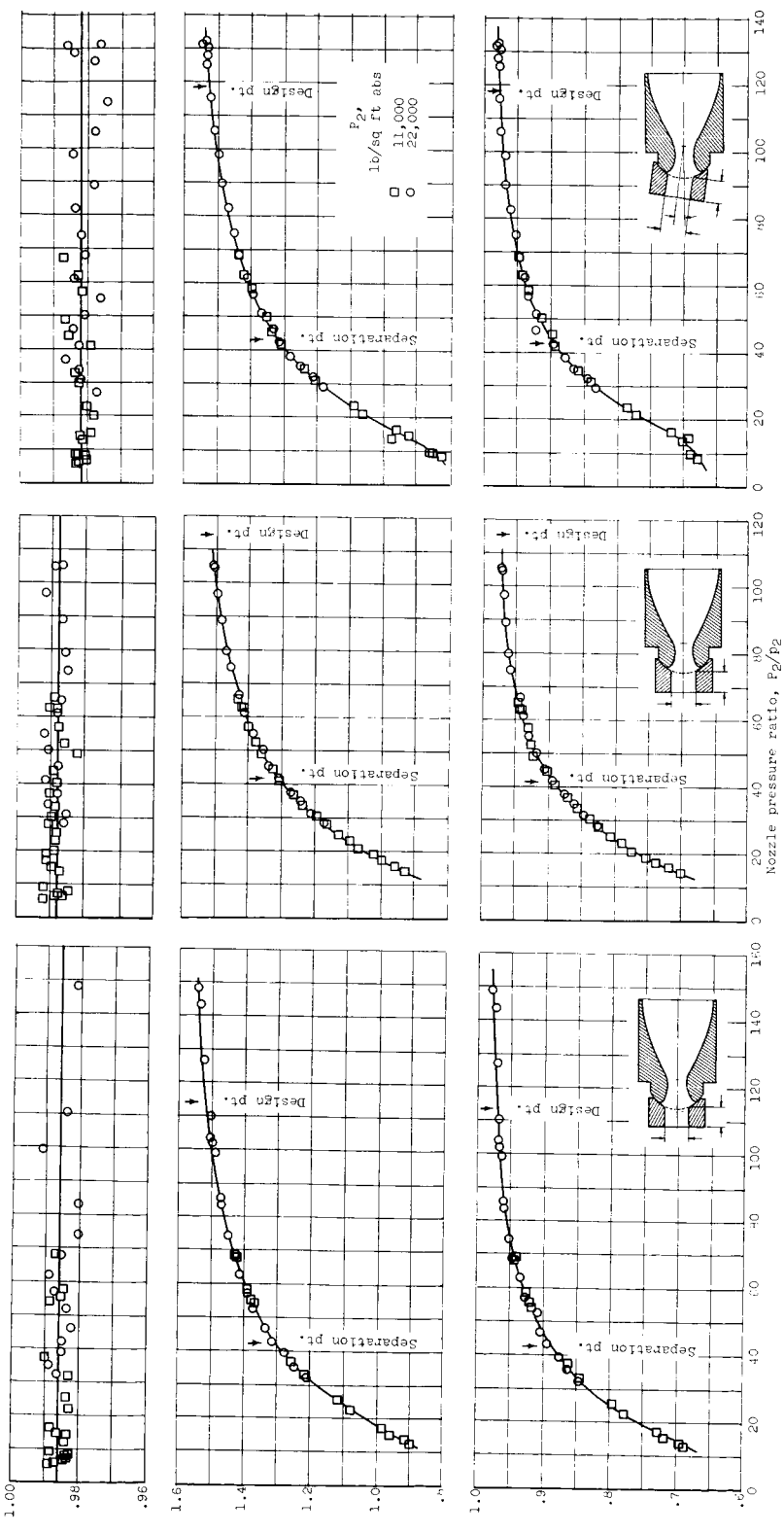

(j) Configuration 10 (0.4-$\frac{1}{2}$-1"R). (k) Configuration 11 (0.4-$\frac{1}{2}$-1/2"R). (l) Configuration 12 (0.4-8°-1"R).

Figure 5. - Continued. Variation of $C_{d,3}$, C_F, and F/F_1 with pressure ratio P_2/p_0.

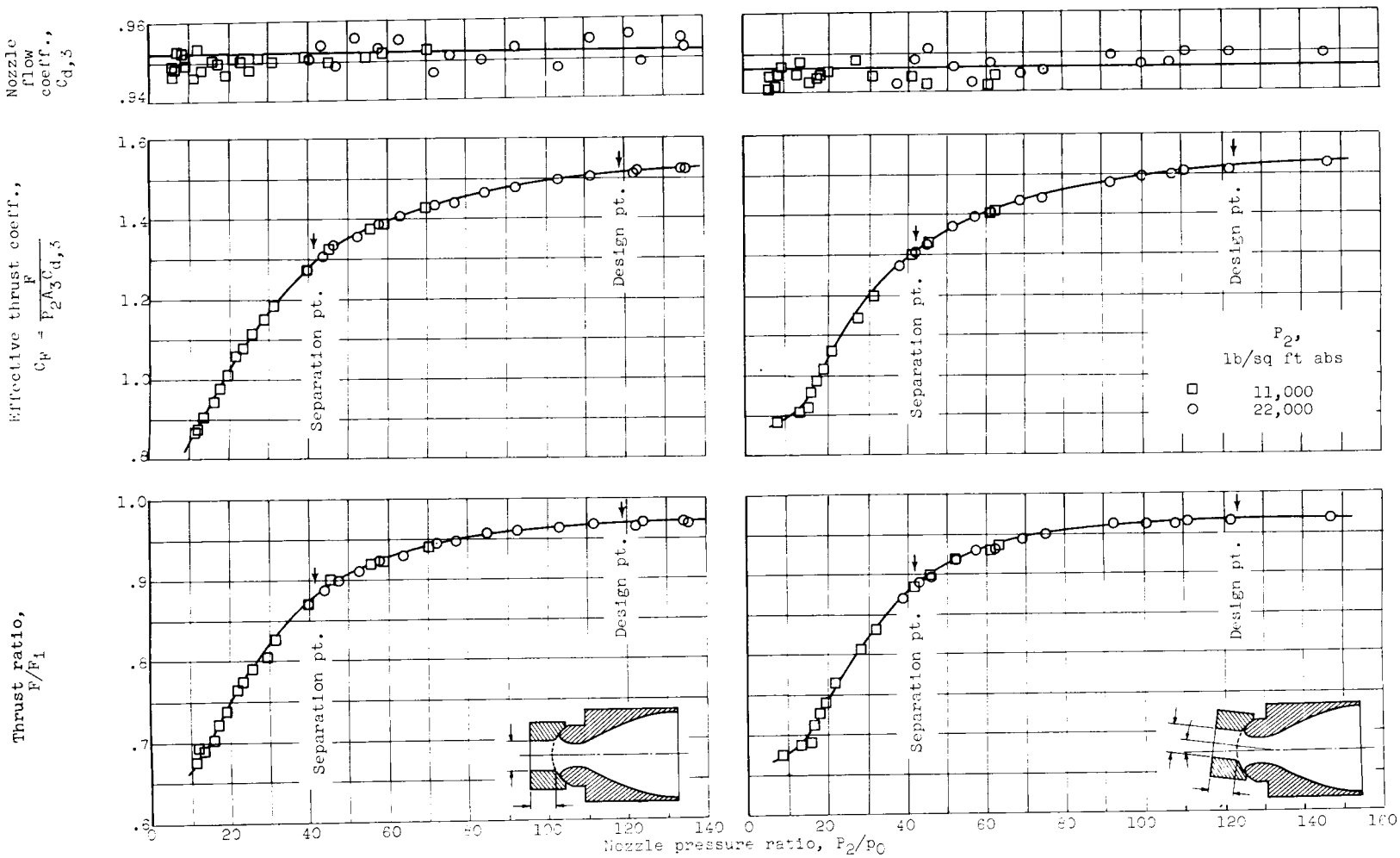

(m) Configuration 13 (0.4-t-Sq.).

(n) Configuration 14 (0.4-8°-Sq.).

Figure 5. - Continued. Variation of $C_{d,3}$, C_F, and F/F_1 with pressure ratio P_2/P_0.

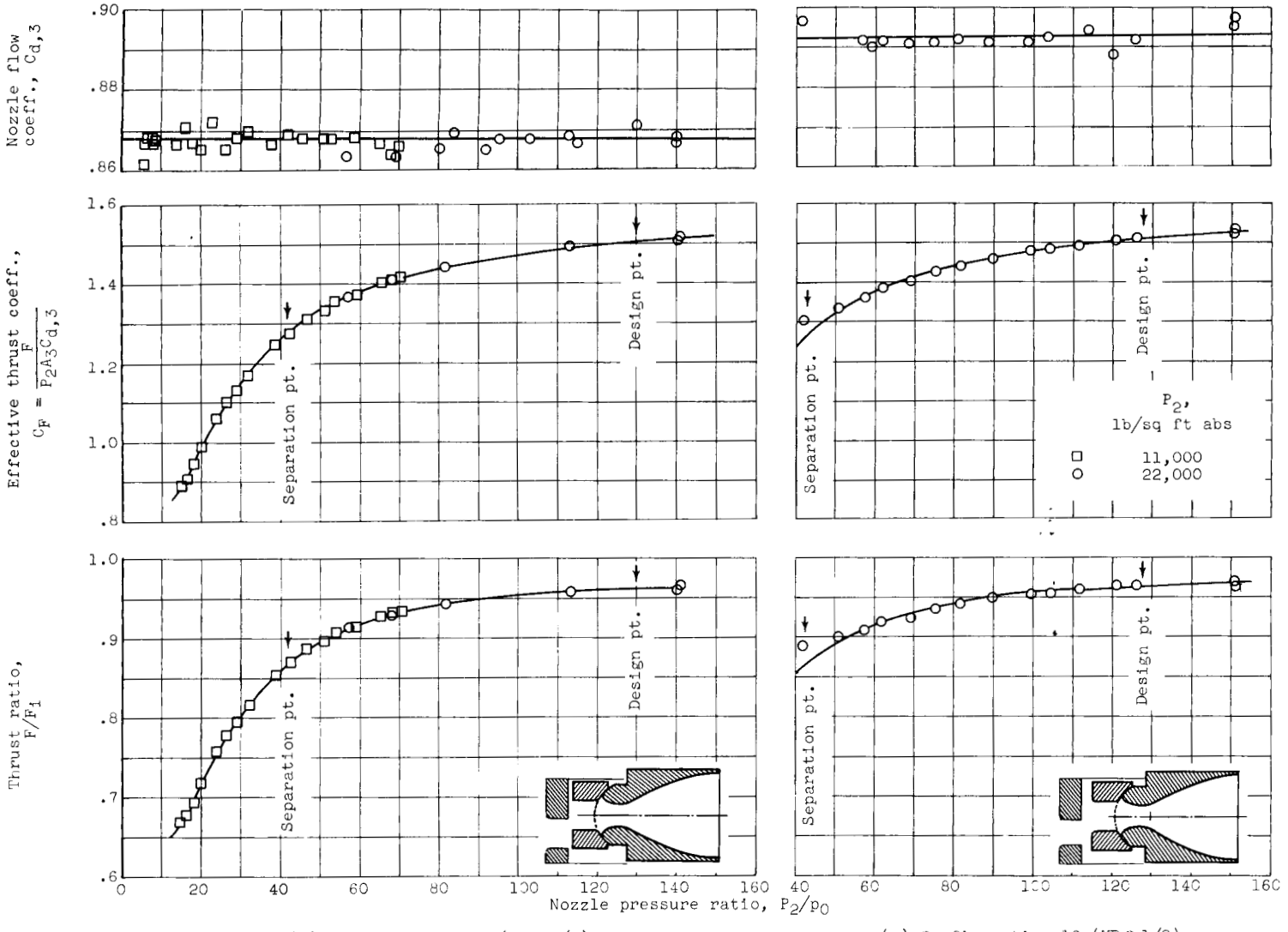

(o) Configuration 15 (MB@ 1/4).

(p) Configuration 16 (MB@ 1/2).

Figure 5. - Continued. Variation of $C_{d,3}$, C_F, and F/F_1 with pressure ratio P_2/p_0.

(q) Configuration 17 (MB @ 1).

(r) Configuration 18 (MB @ 2).

(s) Configuration 19 (MB @ 6).

Figure 5. - Concluded. Variation of $A_{3,2}$, C_F, and F/F_1 with pressure ratio P_2/p_0.

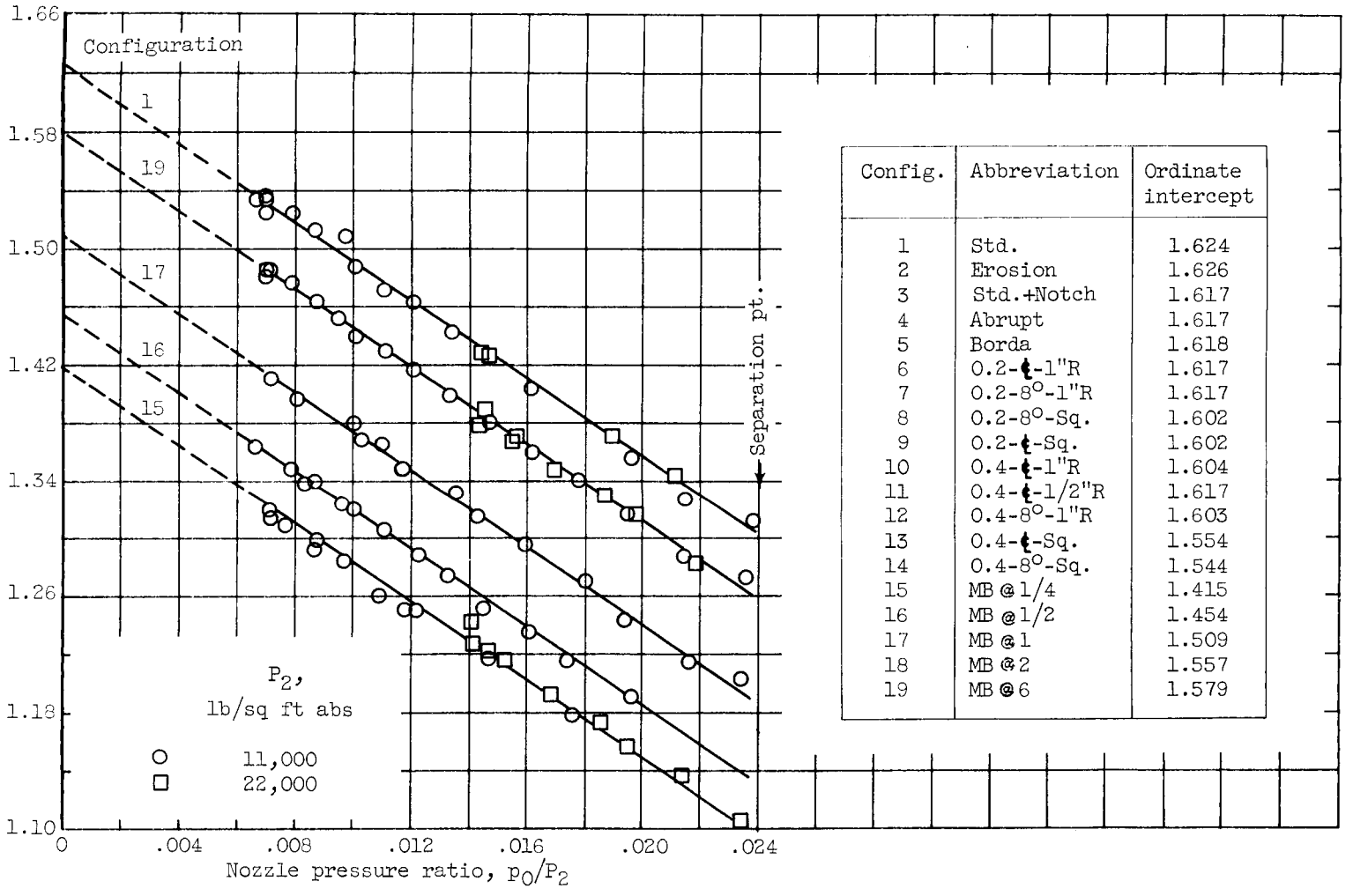

Config.	Abbreviation	Ordinate intercept
1	Std.	1.624
2	Erosion	1.626
3	Std.+Notch	1.617
4	Abrupt	1.617
5	Borda	1.618
6	0.2-℄-1"R	1.617
7	0.2-8°-1"R	1.617
8	0.2-8°-Sq.	1.602
9	0.2-℄-Sq.	1.602
10	0.4-℄-1"R	1.604
11	0.4-℄-1/2"R	1.617
12	0.4-8°-1"R	1.603
13	0.4-℄-Sq.	1.554
14	0.4-8°-Sq.	1.544
15	MB @ 1/4	1.415
16	MB @ 1/2	1.454
17	MB @ 1	1.509
18	MB @ 2	1.557
19	MB @ 6	1.579

Figure 6. - Typical variation of thrust coefficient with pressure ratio.

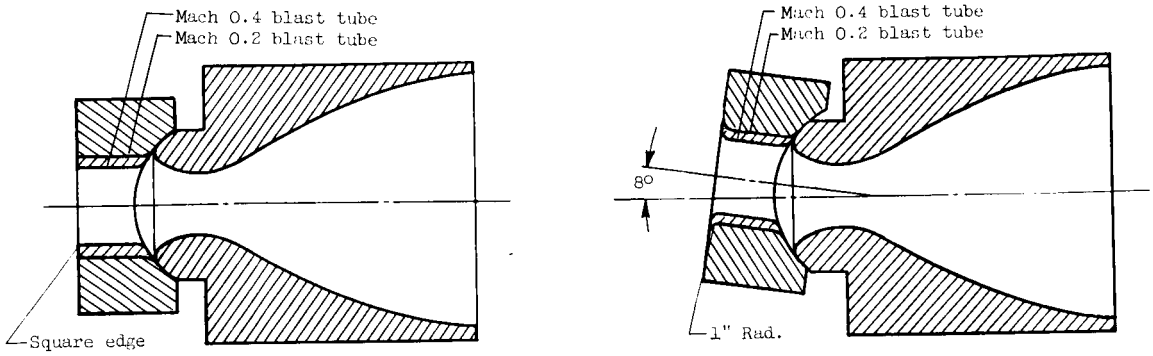

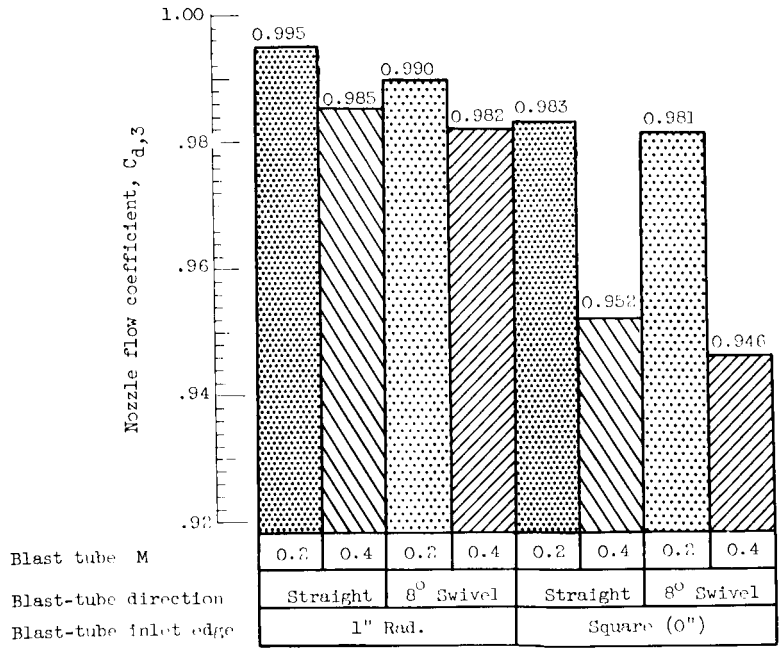

Figure 7. - Effect on nozzle throat flow coefficient of several blast-tube configurations.

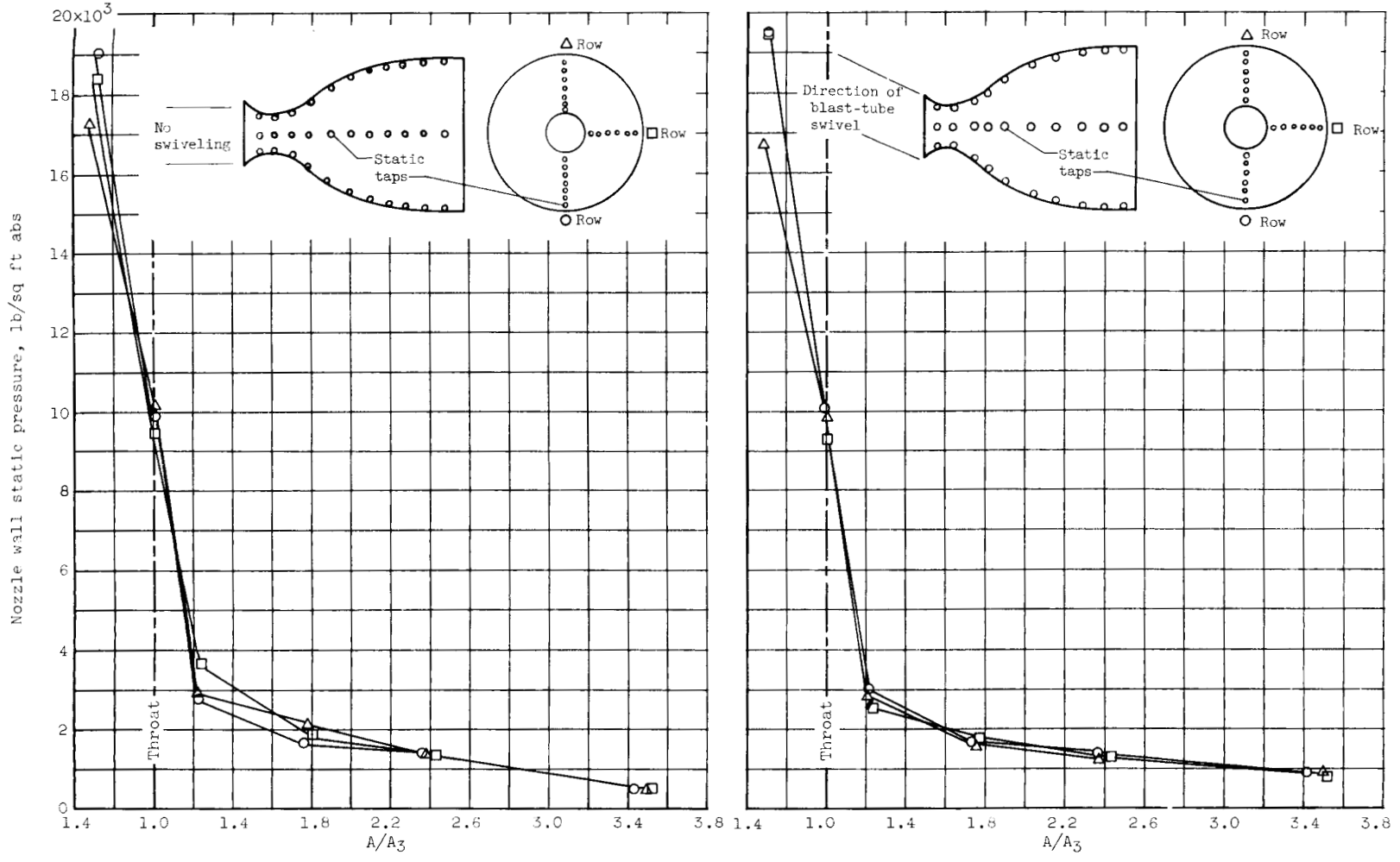

(a) Unswiveled configuration 1 (Std.).

(b) Swiveled configuration 12 (0.4-8°-1"R).

Figure 8. - Static-pressure distributions in divergent section of nozzle.

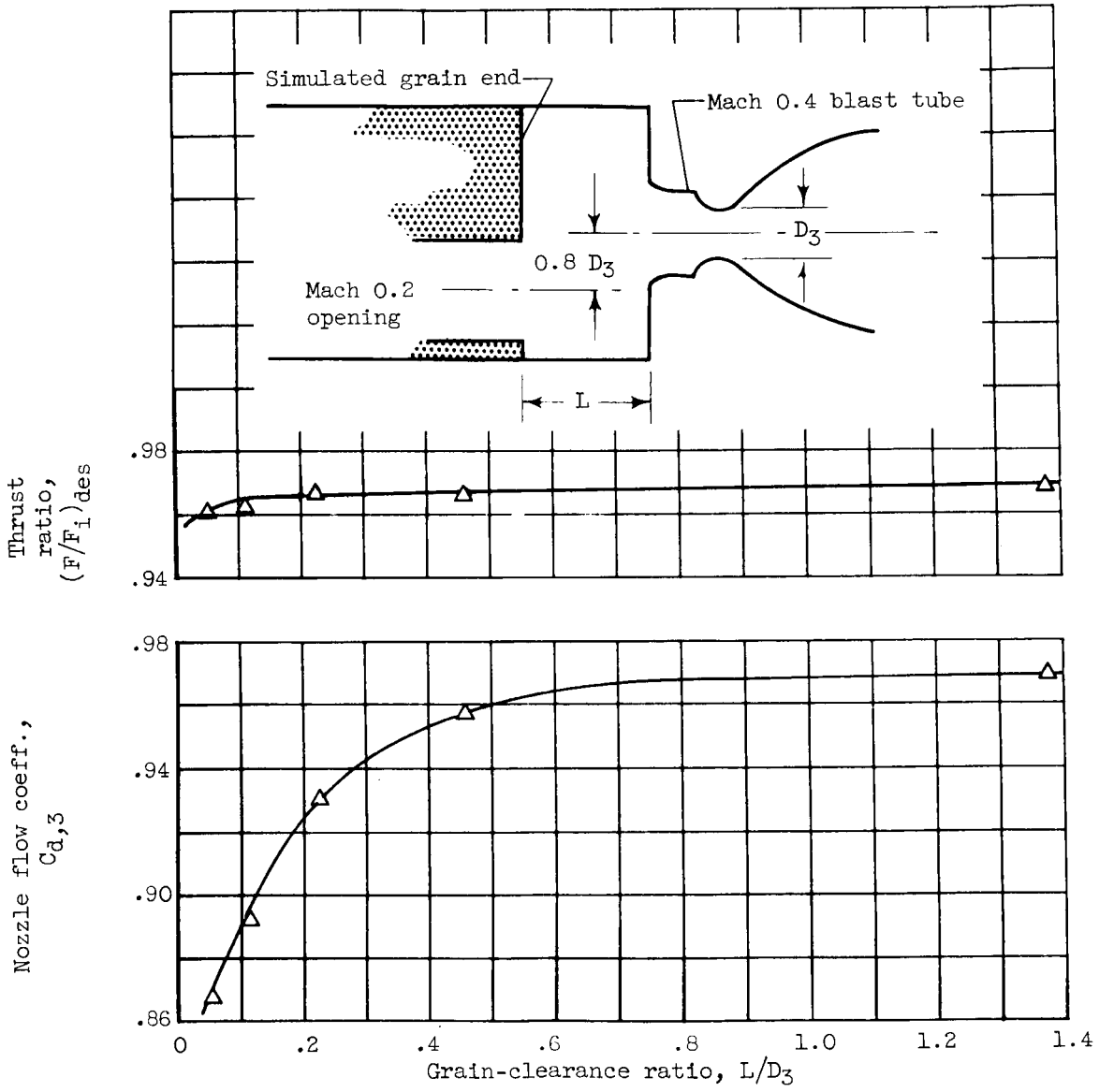

Figure 9. - Effect of grain clearance on nozzle performance.

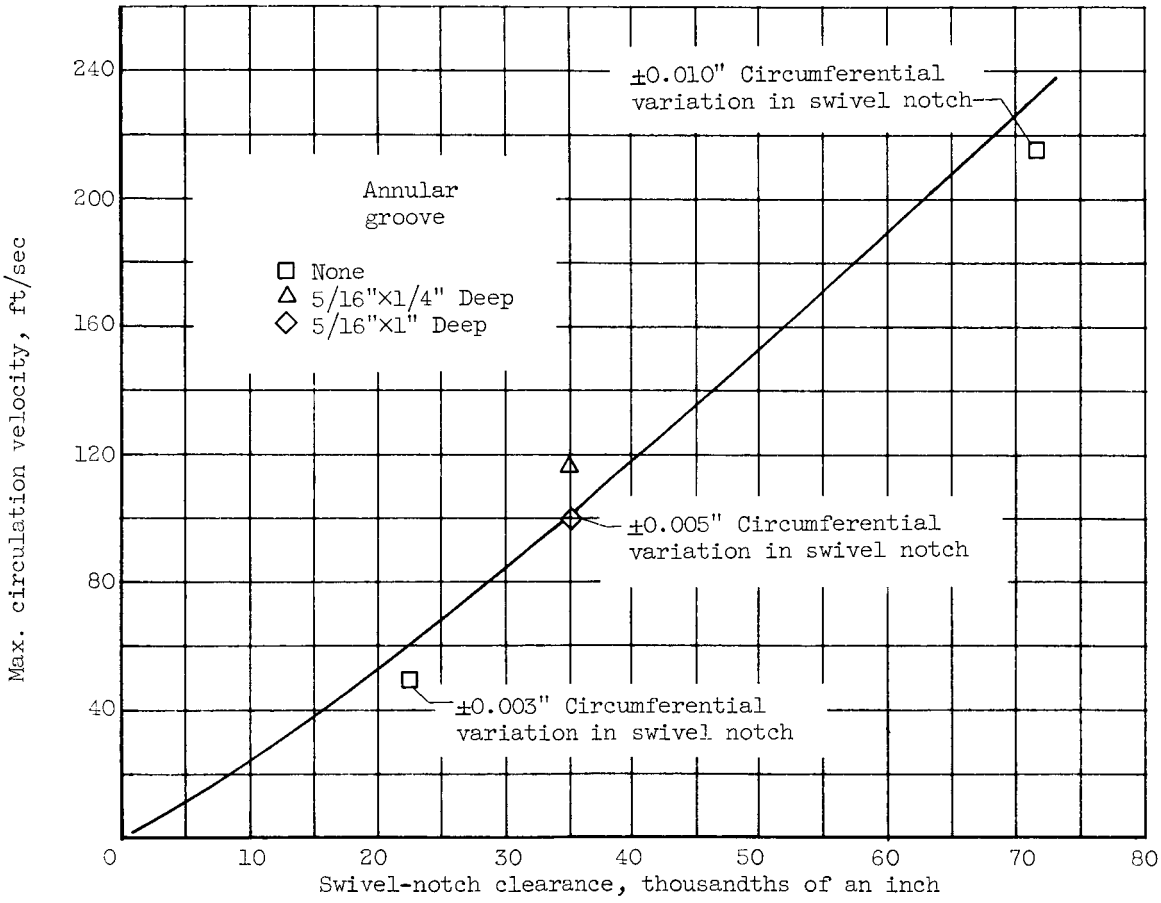

Figure 10. - Effect of swivel-notch clearance on circulation velocity in seal chamber with nozzle choked. Configuration 12 (0.4-8°-1"R).